Mapping Electronic Transport in Ge Nanowire SBFETs: From Tunneling to NDR

1st Raphael Behrle
Institute of Solid State Electronics
TU Wien
Vienna, Austria
raphael.behrle@tuwien.ac.at

2nd Martina Bažíková
Institute of Solid State Electronics
TU Wien
Vienna, Austria
martina.bazikova@tuwien.ac.at

3rd Sven Barth
Institute of Physics
Institute for Inorganic and Analytical Chemistry
Goethe Universität Frankfurt
Frankfurt am Main, Germany
barth@physik.uni-frankfurt.de

4th Walter M. Weber
Institute of Solid State Electronics
TU Wien
Vienna, Austria
walter.weber@tuwien.ac.at

5th Masiar Sistani
Institute of Solid State Electronics
TU Wien
Vienna, Austria
masiar.sistani@tuwien.ac.at

Abstract—An in-depth discussion of the transport mechanisms in ambipolar Ge nanowire (NW) Schottky barrier (SB) field-effect transistors (SBFETs) embedded in monolithic and crystalline Al-Ge-Al heterostructures is presented. Thereto, detailed bias spectroscopy in the temperature regime between T = 77.5 K and 400 K was conducted. In conjunction with the obtained activation energy maps, a highly transparent contact for holes due to charge carrier injection saturation by Fermi level pinning close to the valence band and gate induced thinning of the SB width was observed. In contrast, the thermionic- and field-emission mechanism limits the overall electron conduction, indicating a distinct SB for electrons. In this regime, nanoscaled Ge distinctly differs from its bulk counterpart and delivers a strong and reproducible negative differential resistance (NDR) at room-temperature (RT) followed by a sudden current increase indicating the onset of impact ionization above a specific threshold electric field.

Index Terms—Germanium, Nanowire, Schottky Barrier Field-Effect Transistor, Negative Differential Resistance

I. INTRODUCTION

Low-dimensional Ge structures such as nanowires (NWs) exhibit unique electrical properties [1], [2]. In this respect, the significantly smaller band gap, higher charge carrier mobility of Ge and more prominent quantum effects at larger structural sizes compared to Si are the most important properties for nanoelectronic devices. Further, a highly interesting transport mechanism exhibited by nanoscale Ge is negative differential resistance (NDR) based on the transferred-electron effect, which applies between the L-

and X-valley of the conduction band landscape [3]. So far, this effect was investigated in ultra-thin Ge nanosheets [4], reverse biased Ni/Ge Schottky diodes [5] and Ge NWs [6], [7]. To facilitate these advantages, high-quality and well-defined metal-semiconductor contacts are of utmost importance, as the injection of charge carriers highly depend on the interface and its incorporated energy barrier [8]. In this context, intense research was carried out to achieve Schottky barrier (SB) field-effect transistors (SBFETs) [9] with well defined germanide contacts [10], [11]. However, difficulties in reproducibility and deterministically forming intermetallic phases, led to high device-to-device variability and thus unreliable electrical characteristics [12]. To cope with these limitations, monolithic and single-crystalline Al-Ge junctions [13], [14] with no intermetallic phases were developed. Till now, an in-depth investigation of the electronic transport in Al-Ge-Al heterojunction SBFETs based on detailed bias spectroscopy, providing explanation for their unique electronic properties is still not available. In this regard, we have thoroughly analyzed the temperature dependent electronic transport of single-crystalline Al-Ge-Al NW heterostructure SBFETs.

II. DEVICE ARCHITECTURE

This study is based on vapor-liquid-solid (VLS) Ge NWs grown on a Ge (111) single crystal substrate by low-pressure chemical vapor deposition (CVD) in a cold-wall reactor using an Au metal catalyst and diphenylgermane precursor. Similar growth procedures have been reported in literature [15], [16]. The stability of the synthesized Ge NWs against degradation such as i.e. surface oxidation over time and the formation of reliable interfaces in post-growth processing can be related to surface termination with phenyl ligands originating from the precursor. Source/drain contact formation was carried out by Al deposition and subsequent anneal at 623 K. Al exchanges the adjacent Ge and consequently laterally intrudes into the NW. As previously shown, a monolithic integration of the Ge NWs performing

a thermally induced Al-Ge exchange reaction reveals no intermetallic phases [17]. This device architecture ensures an exceptionally high quality and reproducible fabrication method of metal-semiconductor-metal heterostructures and thus constitutes an ideal platform to study the electronic transport in metal-Ge junctions [13], [18]. Indeed, Fig.1 shows a SEM image of the fabricated Al-Ge-Al NW heterostructure based SBFET with an overlapping Ω-shaped top-gate, consisting of a Ti/Au gate electrode, where the Ti is defining the work function and the Au serves as a bond-pad. To ensure optimal gating capabilities, the used Ge NWs were conformally coated with a $13.5\,\mathrm{nm}$ thick Al_2O_3-shell using atomic layer deposition (ALD) prior to the NW device integration. A schematic illustration of the gate stack is shown in the inset of Fig.1.
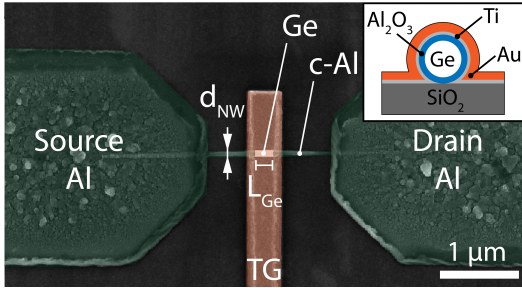

Fig. 1. False color SEM image of a top-gated Al-Ge-Al NW heterostructure with a channel length $L_{Ge} \approx 600\,\mathrm{nm}$ and a diameter $d_{NW} \approx 50\,\mathrm{nm}$. The inset shows a schematic illustration of the cross-section and used gate stack.

III. ROOM-TEMPERATURE TRANSPORT

For basic characterization of the Al-Ge-Al NW heterostructure SBFETs, Fig.2 shows the subthreshold transfer characteristic of a representative device for bias voltages between $V_{DS} = 10\,\mathrm{mV}$ and $200\,\mathrm{mV}$. The measurement was conducted by pulsing V_{TG} with a pulse width of $1\,\mathrm{ms}$, a base of $0\,\mathrm{V}$ and 202 measurement points, minimizing the influence of charge carrier trapping effects (slow traps) [24]. Although the devices are based on intrinsic Ge NWs, a predominant p-type behavior was found. Typical for metal-Ge junctions, strong Fermi level pinning close to the valence band [19], [20] limits the injection capability of electrons and thus only allows weak electron conduction for $V_{TG} > 1\,\mathrm{V}$. This behavior is schematically represented by the band diagram insets. While the on-current for hole conduction at $V_{TG} = -5\,\mathrm{V}$ is tunable with the applied V_{DS}, the electron dominated current for $V_{TG} = 5\,\mathrm{V}$ remains stable at a current density of $J_p \approx 510 \times 10^3\,\mathrm{A/cm^2}$. Most notably, in the hole dominant regime exceptionally high current values normalized to the NW diameter d_{NW} are achieved as depicted on the right axis of Fig.2. Compared to Al-Si-Al NW heterostructure based SBFETs [21], this value is more than a factor 30 higher, which highlights the suitability of Ge for p-type transistors.

IV. TEMPERATURE DEPENDENT TRANSPORT

The different transport regimes are next characterized based on temperature and V_{TG} dependent I_D/V_{DS} measurements. Thereof, two cases can be identified: For distinct
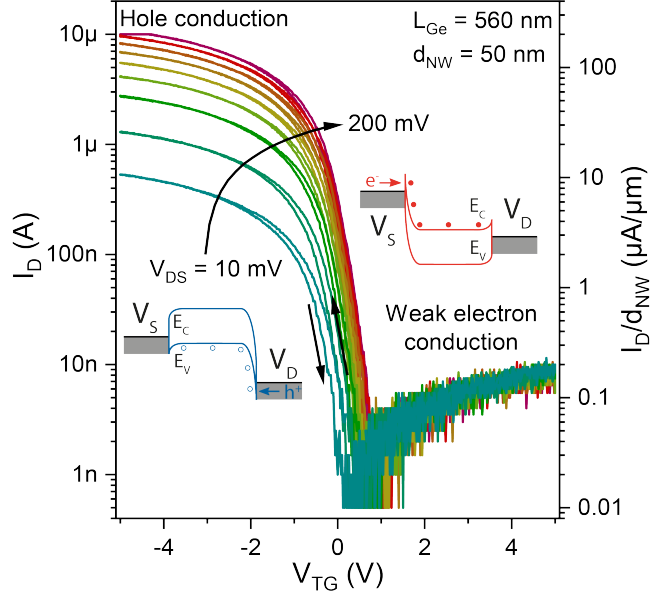

Fig. 2. Typical transfer characteristic of an Al-Ge based SBFET measured by pulsing V_{TG} for V_{DS} between $10\,\mathrm{mV}$ and $200\,\mathrm{mV}$. Thus, only a insignificant hysteresis is evident. The insets depict the band bending mechanism leading to ambipolar FET operation.

injection barriers the Schottky junction resistance is larger than the Ge channel resistance (thermionic emission limited transport). In the case of a thinned, highly transparent junction the resistance of the Schottky junction is smaller compared to the resistance of the Ge channel (field emission limited transport). Evaluating the temperature dependent output characteristic allows to didactically distinguish between the dominant conduction mechanism of a Schottky junction. Thereto, Fig.3 shows the respective color maps of an Al-Ge based SBFET for $T = 77.5\,\mathrm{K}$, $T = 295\,\mathrm{K}$ and $T = 400\,\mathrm{K}$. As shown in the inset of Fig.3a, the operation of an ambipolar SBFET is usually governed by thermionic (TE), thermionic-field (TFE) and field emission (FE). Note that, TFE is a mixed transport regime, where both TE and FE contribute essentially to the charge carrier injection. Comparing the output maps reveals that increasing the temperature up to room-temperature (RT), the TE region (dark blue) is strongly reduced, while the TFE (light green) is increasing and the FE region (yellow) remains relatively stable. As TE in the electron dominant regime ($V_{TG} >> 0\,\mathrm{V}$) is given by the SB height, which in the Al-Ge system is substantially higher for electrons than for holes, the thermal excitation highly contributes to TE at elevated temperatures. In contrast, FE and its transmission probability can be described for didactic simplicity by the Wenzel-Kramers-Brillouin (WKB) approximation of a triangular barrier shape: $T \approx \exp\left(\frac{4\sqrt{2m^*}\phi^{3/2}}{3q\hbar\mathcal{E}}\right)$, where m^* is the charge carrier's tunneling effective mass, ϕ the energy barrier height, q the elementary charge and $\mathcal{E}$ the electric field across the junction that actually sets the barrier width. Importantly, FE is a temperature-independent mechanism and therefore remains stable over the observed temperature regime. This observation indicates that temperature independent FE through a thinned SB is the dominant

mechanism contributing to the conduction, especially for holes due to the highly hole-transparent contact properties.
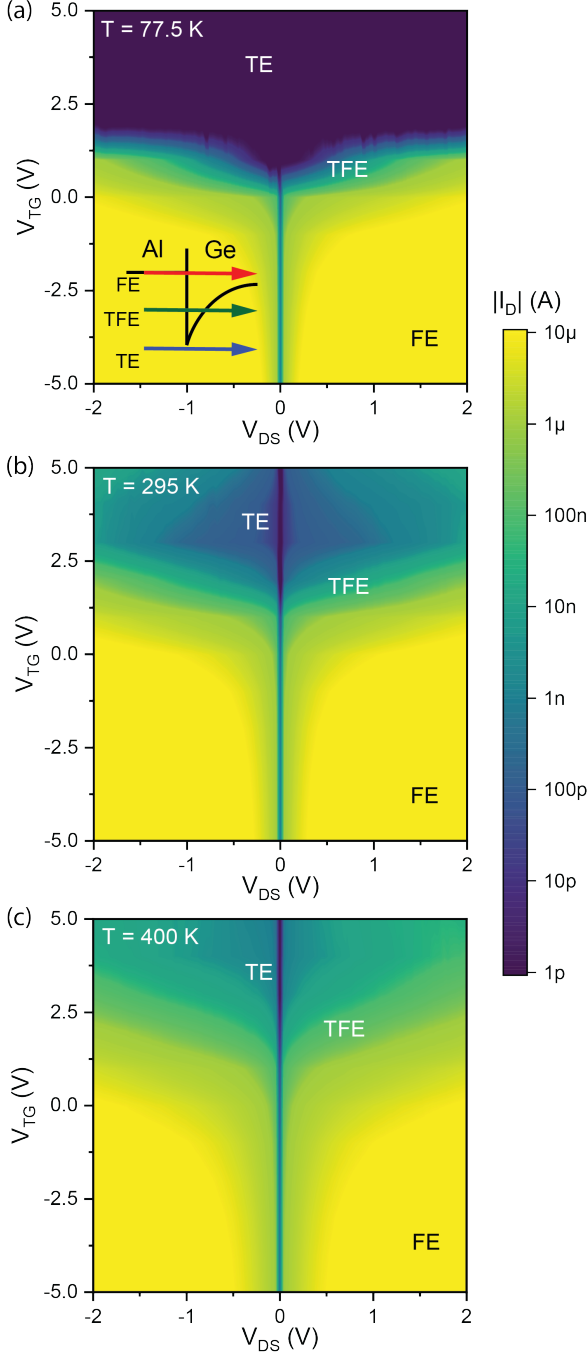

Fig. 3. Output characteristic maps of an Al-Ge based SBFET recorded for temperatures of (a) $T = 77.5$ K, (b) $T = 295$ K and (c) $T = 400$ K. The inset in (a) is didactically showing the dominant transport mechanisms of the Al-Ge Schottky junction.

Fig.4 shows the linear representation of the output characteristic at different V_{TG} values ranging from 2 V to -5 V and sweeping the bias voltage V_{DS} from 0 V to -2 V, clearly revealing the electrostatic gating capabilities of hole conduction in the p-type operation. Moreover, analyzing the output characteristic over temperature of the proposed Al-Ge based SBFET in more depth allows to extract V_{TG}-dependent activation energies [22]. This allows to give

physical quantities in terms of charge carrier injection capabilities, required to extract optimal operation points for individual applications.
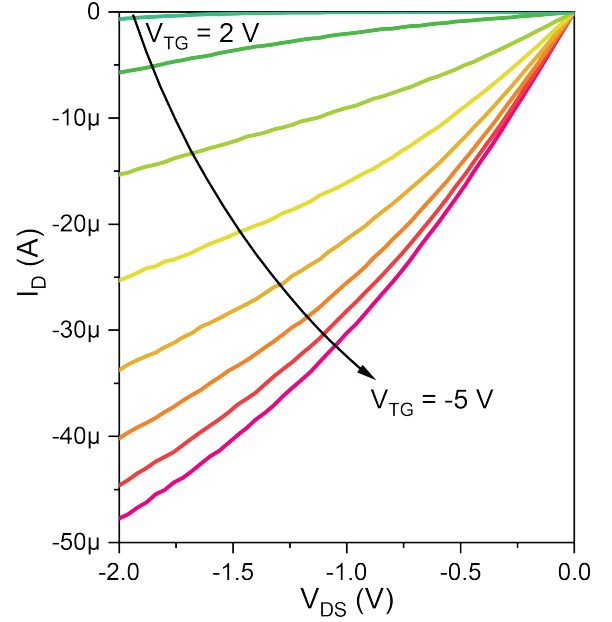

Fig. 4. Linear V_{TG}-dependent output characteristics of the Al-Ge based SBFET. Performing temperature dependent measurements, allows to extract the V_{TG}-dependent E_a.

For the extraction of the activation energy E_a, an experimental model was used, which is deduced from thermionic emission theory, where the temperature dependent current injection density is $J_{TE}(T) = A^* T^2 \exp \frac{-E_a}{k_B T}$. Using this equation, FE, TFE and TE contributions to the total current cannot be separated. However, the mentioned equation gives an estimation of the thereof extracted activation energy. Plotting $\ln \frac{J_{TE}}{T^2}$ vs. $1000/T$ (Arrhenius plot) and evaluating the slope allows to finally extract the activation energy by extrapolating to $V_{DS} = 0$ V. As shown in Fig.5, negative activation energies are estimated in the strong hole dominant transport regime (cf. $V_{TG} = -5$ V), further supporting the evidence of hole-transparent Al-Ge junctions for sufficient barrier thinning ($V_{TG} << 0$). In contrast, operating the device in the electron dominant regime, e.g. $V_{TG} = 5$ V, a dedicated positive but V_{TG}-tunable barrier is evident. Remarkably, the off-point correlates well with the obtained transfer characteristic (cf. Fig.2 and Fig.6), with a maximum estimated activation energy of $E_a = 0.66$ eV, which matches with the band gap energy of Ge.

Fig.6 shows the temperature dependent transfer characteristic for applying $V_{DS} = 1$ V. Due to more effective channel depletion by charge carrier freeze-out at $T = 77.5$ K, a remarkably high on/off ratio of I_D of more than eight orders of magnitude is observed. Consequently, upon heating, the off-current is significantly increasing from 70 fA at 77.5 K (noise floor of the used equipment) to 30 nA at 400 K, reducing the steepness of the transfer characteristic as well as initiating a threshold voltage V_{th} shift (see inset). Up to RT the on-current was found to be increasing due to thermally driven TE. Interestingly, a
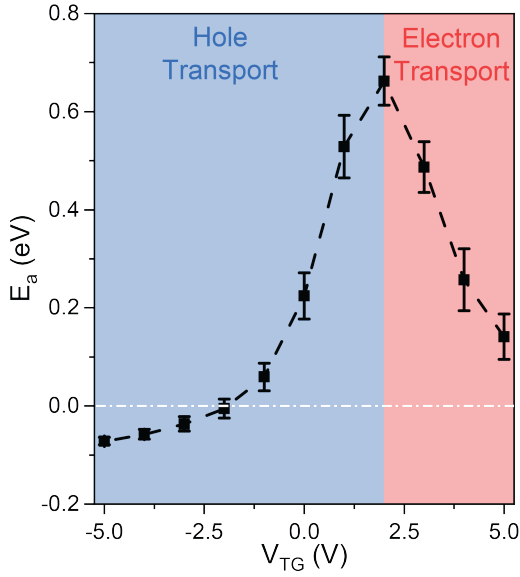
Fig. 5. E_a as a function of V_{TG}, indicating a highly transparent junction for holes and a distinct barrier for electrons. Error bars were deduced from measurements of three similar SBFETs.

Fig. 6. Transfer characteristics of the proposed Al-Ge SBFET recorded for temperatures between $77.5\,\mathrm{K}$ and $400\,\mathrm{K}$ and a bias voltage of V_{DS} = $1\,\mathrm{V}$. The inset depicts a cubic fitted thermally induced V_{th} shift typical for SBFETs. V_{th} was extracted using the linear transconductance interpolation method.

further increase of the temperature results in decreasing on-currents at $V_{TG} = -5\,\mathrm{V}$. This is an indication that the contact resistance of the Schottky junction becomes less significant compared to the resistance of the Ge channel. Remarkably, in this regime the on-current merely varies between $24\,\mu\mathrm{A}$ ($400\,\mathrm{K}$) and $33\,\mu\mathrm{A}$ ($225\,\mathrm{K}$). In agreement with the findings of the temperature dependent output characterization phonon scattering is the dominant mechanism contributing to the resistance [23]. In return this is a strong argument for a thinned barrier with a high tunneling probability, giving a quasi-ohmic, i.e. highly transparent junction for holes. In contrast, the weak electron dominated current observed for $V_{TG} = 5\,\mathrm{V}$ is continuously increasing with temperature, indicating a distinct SB for electrons. Here, the on-currents are in the range of $10\,\mathrm{pA}$ ($77.5\,\mathrm{K}$) and $80\,\mathrm{nA}$ ($400\,\mathrm{K}$). Consequently, in this regime, TE limited conduction with the contact resistance being the dominant contributor to the overall device resistance is expected.

To investigate the charge carrier trapping behavior of the proposed Al-Ge SBFET devices, Fig.7 shows the temperature dependent transfer characteristics measured under pulsed V_{TG} condition to exclude charging effects due to the substrate of the chip ($1\,\mathrm{ms}$, base voltage of $0\,\mathrm{V}$, 202 measurement points). An insignificant hysteresis up to $350\,\mathrm{K}$ indicates a reduced density of trap states compared to more common Ge NW devices based on GeH_4 precursors [24]. Importantly, the on-state currents as well as threshold voltages of the individual temperature-dependent curves are in accordance with continuous measurements (cf. Fig.6) without significant differences. However, a minor hysteresis is evident at the intrinsic point, i.e. V_{TG} at off-current of the transfer characteristic, which is most likely attributed to thermally excited charge carriers, i.e. TE over the SB. Further, the hysteresis in the p-branch might be attributed to the recombination of trapped electrons.

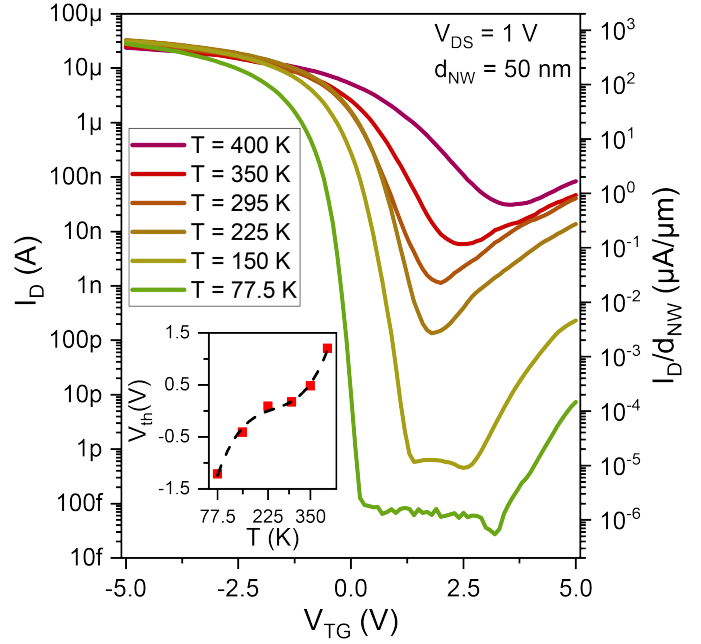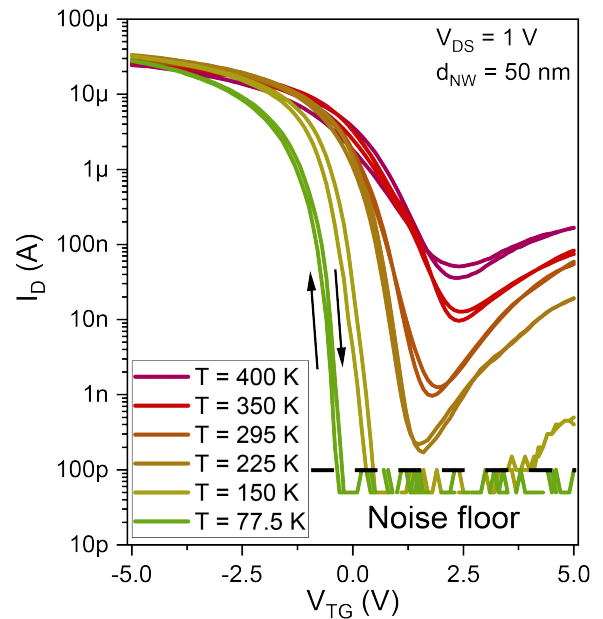Extracting the transconductance g_m of the temperature

Fig. 7. Transfer characteristics measured under pulsed V_{TG} condition recorded for temperatures between $77.5\,\mathrm{K}$ and $400\,\mathrm{K}$ and a bias voltage of $V_{DS} = 1\,\mathrm{V}$. Up to $350\,\mathrm{K}$ no substantial hysteresis is evident.

dependent transfer characteristics reveals a degradation for increasing T in the hole dominant regime. Remarkably, as shown in Fig.8, this effect appeared to be bias and temperature independent in the regime of strong accumulation. This is contrary to common SBFETs with a distinct injection barrier, where the transconductance g_m (except for applying a high V_{DS}) is continuously enhanced for an increasing gate bias [22]. While origins of g_m degradation also involve surface roughness scattering and series resistances [25], a saturation of hole injection due to strong Fermi level pinning to the valence band and efficient carrier injection through the thin SB appears to be the dominant factor. Thus, in agreement with the gate-dependent activation energy extraction, a highly transparent, i.e. quasi-ohmic junction with phonon scattering in the Ge channel is the most probable mechanism degrading g_m. In accordance with an increasing scattering mean free path, i.e. reduced phonon scattering at lower temperatures, g_m was found to significantly increase from approximately $2.7\,\mu S$ at $T = 400\,K$ to about $5.8\,\mu S$ at $T = 77.5\,K$.
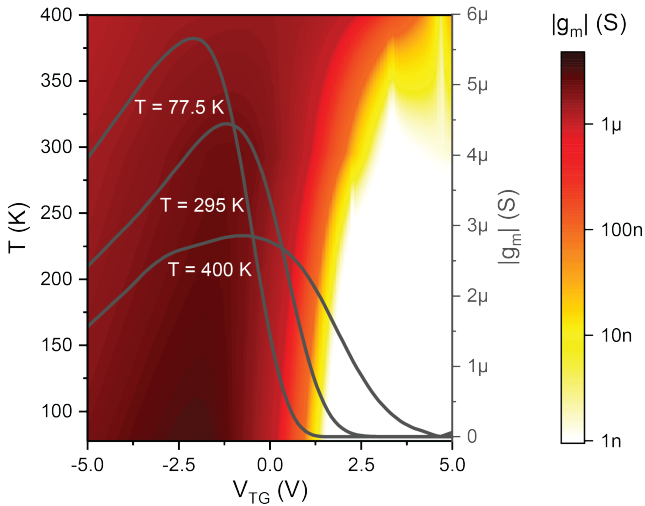

Fig. 8. Transconductance map plotted over temperature with distinctly high values in the p-type regime. On the right y-axis (gray curves) $|g_m|$ values for applying $V_{DS} = 1\,V$ are plotted for $T = 77.5\,K$, $295\,K$ and $400\,K$.

V. Temperature dependent NDR

Operating the Al-Ge based SBFETs at high electric fields in the electron dominated regime, the combined influences of electrostatic gating and geometric confinement seem to provide an efficient hot electron transfer effect, enabling distinct NDR in Ge, even at RT. Importantly, due to time-stable measurement conditions related to the use of the diphenylgermane precursor for NW growth, the electronic transport mechanisms and especially NDR can be investigated in terms of the manifold influencing parameters, i.e. bias voltages, as well as from a temperature-dependent point of view. In this regard, Fig.9 shows an $log_{10}|I_D|/V_{DS}$ measurement at $T = 77.5\,K$. Thereof, four distinct slopes can be identified, which can be assigned to: S1: TE, S2: TFE (cf. Fig.3a), S3: electron transfer from the L- to the X-valley in the conduction band constituting a significant

mobility decrease resulting in NDR (cf. lower inset) and S4: impact ionization (II) by an avalanche-like increase of electrons at high electric fields as sketched in the upper inset. The subsequent flattening of the slope after II might be due to self-heating.
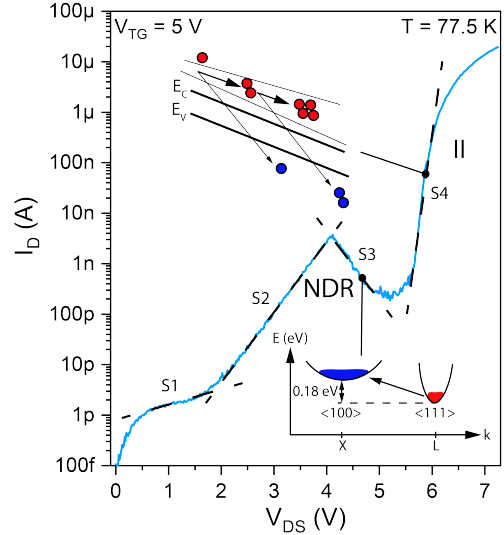

Fig. 9. NDR I/V characteristic at $V_{TG} = 5\,V$ recorded at $T = 77.5\,K$. The slopes S denote the different transport regimes. The upper inset shows a schematic illustration of II due to a hot-electron induced avalanche. The lower inset shows the electron transfer from the L- to the X-valley resulting in NDR.

Fig.10 shows temperature dependent $log_{10}I_D/V_{DS}$ measurements to depict the evolution of NDR as a function of temperature. Due to thermal activation, a temperature related peak- and valley-shift (V_p and V_v) to lower V_{DS} is observed for increasing temperatures. A shift of $8.5\,mV/K$ was detected for both, V_p and V_v. Importantly, still maintaining a peak-to-valley ratio of 5, a stable and reproducible NDR was observed up to temperatures of $T = 350\,K$, which is an important requirement for actual implementations of NDR-based logic applications. Beyond this temperature, the NDR effect vanished due to thermally activated transport in the L-valley and a strongly decreased scattering efficiency from the L- to the X-valley.

VI. Conclusion

The temperature dependent charge carrier transport in Al-Ge SBFETs with single-crystalline Al contacts by means of bias spectroscopy has been analyzed. Highlighting the suitability for p-type transistors, exceptionally high current values of $I_D/d_{NW} = 200\,\mu A/\mu m$ for relatively low bias voltages of $V_{DS} = 200\,mV$ are achieved. Contrary to common SBFETs with a distinct injection barrier, the thereof extracted activation energies and temperature dependent transfer characteristics revealed a highly transparent contact for holes due to charge carrier injection saturation by Fermi level pinning close to the valence band and a thinned SB in strong accumulation. In contrast, TE limited electron conduction over a distinct SB for electrons was found. Importantly, the bias spectroscopy maps of I_D, g_m and E_a reveal the operation regimes and underlying
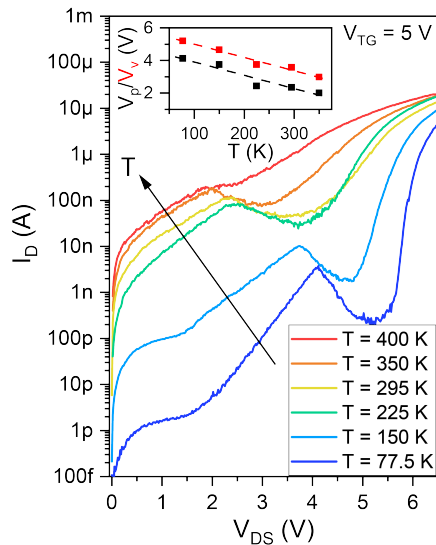
Fig. 10. Temperature dependent NDR measurements for $V_{TG} = 5\,\mathrm{V}$. The inset shows the temperature dependent evolution of V_p and V_v indicating a thermally induced linear voltage downshift with increasing temperatures. A linear fit of the data was inserted as a guide for the eye.

transport properties of modern Ge NW SBFETs with crystalline and monolithic Al contacts, opening new paths for RT operability of NDR-based Ge devices fabricated by top-down fabrication schemes [26].

REFERENCES

[1] R. Pillarisetty, "Academic and industry research progress in germanium nanodevices," Nature, vol. 479, no. 7373. Nature Publishing Group, pp. 324–328, Nov. 17, 2011.

[2] W. M. Weber and T. Mikolajick, "Silicon and germanium nanowire electronics: Physics of conventional and unconventional transistors," Reports on Progress in Physics, vol. 80, no. 6, p. 066502, Jun. 2017.

[3] C. Jacoboni et al., "Electron Drift Velocity and Diffusivity in Germanium," Physical Review B, vol. 24, pp. 1014–1026, Jul. 1981.

[4] D. Kazazis, A. Zaslavsky, E. Tutuc, N. A. Bojarczuk, and S. Guha, "Negative differential resistance in ultrathin Ge-on-insulator FETs," Semiconductor Science and Technology, vol. 22, no. 1, pp. S1–S4, Nov. 2006.

[5] M. Husain, X. V. Li, and H. de, "Observation of Negative Differential Conductance in a Reverse-Biased Ni/Ge Schottky Diode," IEEE Electron Device Letters, vol. 30, no. 9, pp. 966–968, Sep. 2009.

[6] F. Brunbauer, E. Bertagnolli, and Alois Lugstein, "Gate-Tunable Electron Transport Phenomena in Al–Ge⟨111⟩–Al Nanowire Heterostructures," Nano Letters, vol. 15, no. 11, pp. 7514–7518, Oct. 2015.

[7] R. Böckle et al., "Gate-Tunable Negative Differential Resistance in Next-Generation Ge Nanodevices and their Performance Metrics," Advanced Electronic Materials, vol. 7, no. 3, p. 2001178, Jan. 2021.

[8] A. Thanailakis and D. C. Northrop, "Metal-germanium Schottky barriers," Solid State Electron, vol. 16, no. 12, pp. 1383–1389, Dec. 1973.

[9] M. Schwarz et al., "The Schottky barrier transistor in emerging electronic devices," Nanotechnology, vol. 34, no. 35, pp. 352002–352002, Jun. 2023.

[10] Y.-L. Chao, Y. Xu, R. Scholz, and J. C. S. Woo, "Characterization of copper germanide as contact metal for advanced MOSFETs," IEEE Electron Device Letters, vol. 27, no. 7, pp. 549–551, Jul. 2006.

[11] N. S. Dellas, S. Minassian, J. M. Redwing, and S. E. Mohney, "Formation of nickel germanide contacts to Ge nanowires," Appl Phys Lett, vol. 97, no. 26, p. 263116, Dec. 2010.

[12] J. Trommer et al., "Enabling Energy Efficiency and Polarity Control in Germanium Nanowire Transistors by Individually Gated Nanojunctions," ACS Nano, vol. 11, no. 2, pp. 1704–1711, Feb. 2017.

[13] S. Kral et al., "Abrupt Schottky Junctions in Al/Ge Nanowire Heterostructures," Nano Lett, vol. 15, no. 7, pp. 4783–4787, Jul. 2015.

[14] K. El Hajraoui et al., "In Situ Transmission Electron Microscopy Analysis of Aluminum–Germanium Nanowire Solid-State Reaction," Nano Lett, vol. 19, no. 5, pp. 2897–2904, May 2019.

[15] M. Sistani et al., "Nanoscale aluminum plasmonic waveguide with monolithically integrated germanium detector," Applied Physics Letters, vol. 115, no. 16, Oct. 2019.

[16] S. Barth et al., "Localized growth and in situ integration of nanowires for device applications," Chemical Communications, vol. 48, no. 39, pp. 4734–4736, Apr. 2012.

[17] K. El Hajraoui et al., "In Situ Transmission Electron Microscopy Analysis of Aluminum–Germanium Nanowire Solid-State Reaction," Nano Letters, vol. 19, no. 5, pp. 2897–2904, Mar. 2019.

[18] M. Sistani et al., "Plasmon-Driven Hot Electron Transfer at Atomically Sharp Metal-Semiconductor Nanojunctions," ACS Photonics, vol. 7, no. 7, pp. 1642–1648, Jul. 2020.

[19] Y. Zhou, M. Ogawa, X. Han, and K. L. Wang, "Alleviation of Fermi-level pinning effect on metal/germanium interface by insertion of an ultrathin aluminum oxide," Appl Phys Lett, vol. 93, no. 20, p. 202105, Nov. 2008.

[20] R. Clark, "Emerging Applications for High-k Materials in VLSI Technology," Materials, vol. 7, no. 4, pp. 2913–2944, Apr. 2014.

[21] L. Wind et al., "Monolithic and Single-Crystalline Aluminum-Silicon Heterostructures," ACS Appl Mater Interfaces, vol. 14, no. 22, pp. 26238–26244, Jun. 2022.

[22] D.-Y. Jeon et al., "In-depth electrical characterization of carrier transport in ambipolar Si-NW Schottky-barrier FETs," in 2017 47th European Solid-State Device Research Conference (ESSDERC), Sep. 2017, pp. 304–307.

[23] J. Svensson and E. E. B. Campbell, "Schottky barriers in carbon nanotube-metal contacts," J Appl Phys, vol. 110, no. 11, p. 111101, Dec. 2011.

[24] M. Sistani, P. Staudinger, and Alois Lugstein, "Polarity Control in Ge Nanowires by Electronic Surface Doping," Journal of Physical Chemistry C, vol. 124, no. 36, pp. 19858–19863, Aug. 2020.

[25] D. Y. Jeon et al., "Scaling and Graphical Transport-Map Analysis of Ambipolar Schottky-Barrier Thin-Film Transistors Based on a Parallel Array of Si Nanowires," Nano Lett, vol. 15, no. 7, pp. 4578–4584, Jul. 2015.

[26] L. Wind et al., "Monolithic Metal–Semiconductor–Metal Heterostructures Enabling Next-Generation Germanium Nanodevices," ACS Applied Materials & Interfaces, vol. 13, no. 10, pp. 12393–12399, Mar. 2021.